AGGREGATES AND SUPERAGGREGATES OF SOOT WITH FOUR DISTINCT FRACTAL MORPHOLOGIES

C.M. Sorensen, W. Kim, D. Fry, and A. Chakrabarti
Department of Physics
Kansas State University
Manhattan, KS 66506

Soot formed in laminar diffusion flames of heavily sooting fuels evolves through four distinct growth phases which give rise to four distinct aggregate fractal morphologies. These results were inferred from large and small angle static light scattering from the flames, microphotography of the flames, and analysis of soot sampled from the flames. The growth stages occur approximately over five successive orders of magnitude in aggregate size. Computer simulations can reproduce the kinetics observed in aggregation and aerogelation of soot clusters and indicate that these four growth stages involve either diffusion limit aggregation or percolation in either three or two dimensions.

Aggregates and Superaggregates of Soot with Four Distinct Fractal Morphologies

C.M. Sorensen, W. Kim, D. Fry, and **A. Chakrabarti**

Department of Physics
Kansas State University
Manhattan, KS 66506-2601

Abstract

Soot formed in laminar diffusion flames of heavily sooting fuels evolves through four distinct growth stages which give rise to four distinct aggregate fractal morphologies. These results were inferred from large and small angle static light scattering from the flames, microphotography of the flames, and analysis of soot sampled from the flames. The growth stages occur approximately over four successive orders of magnitude in aggregate size. Comparison to computer simulations suggests that these four growth stages involve either diffusion limited cluster aggregation or percolation in either three or two dimensions.

Fig.1 Diagram of the small angle and large angle light scattering apparatus. These apparatii allow us to probe soot morphologies from 70 nm to nearly 60 μm.

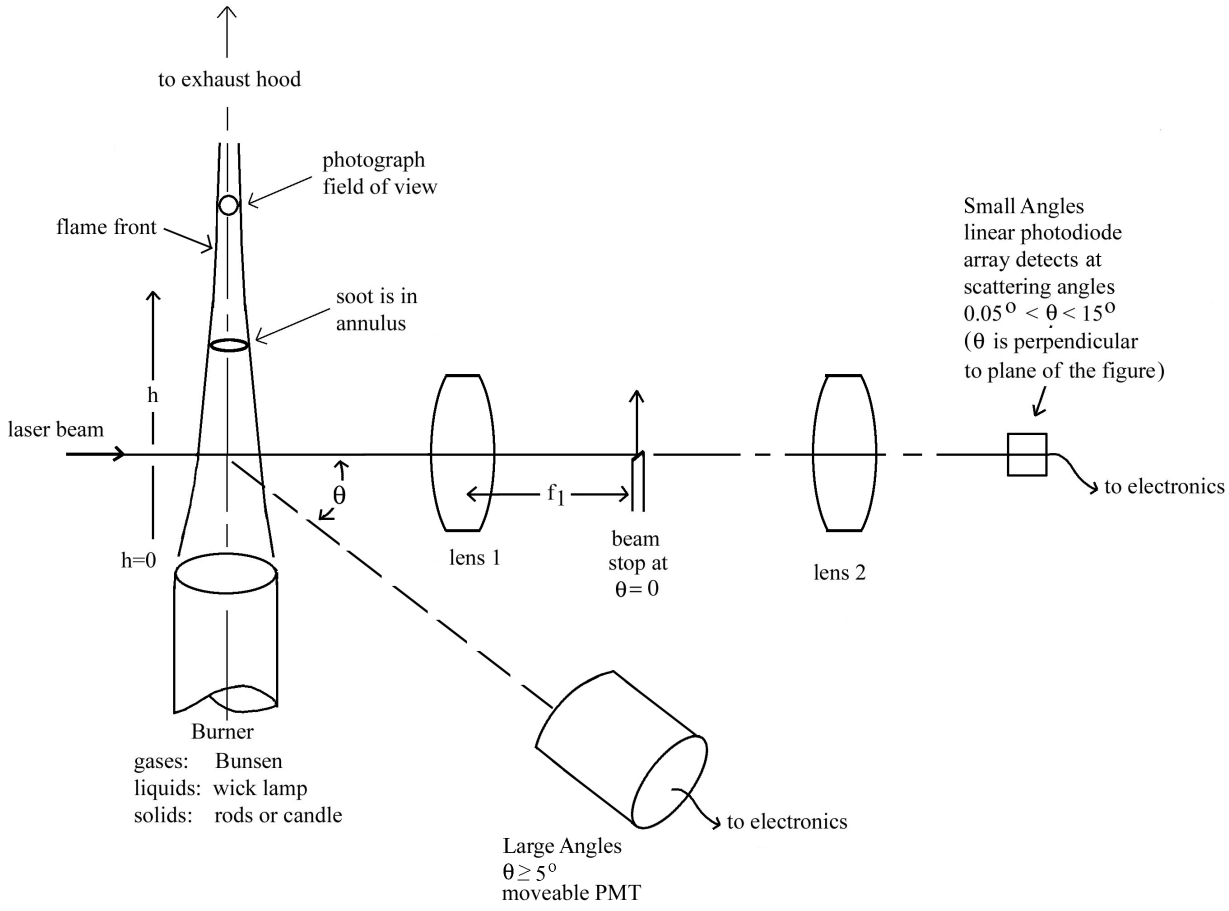

Fig. 2 Scattered Intensity as a function of wavevector, I(q), for an acetylene flame for various heights h above the burner.

Note the presence of: D ≃1.8 aggregates with size ~ 0.3 μm and
D ≃2.6 aggregates with size ~ 12 μm at large h.

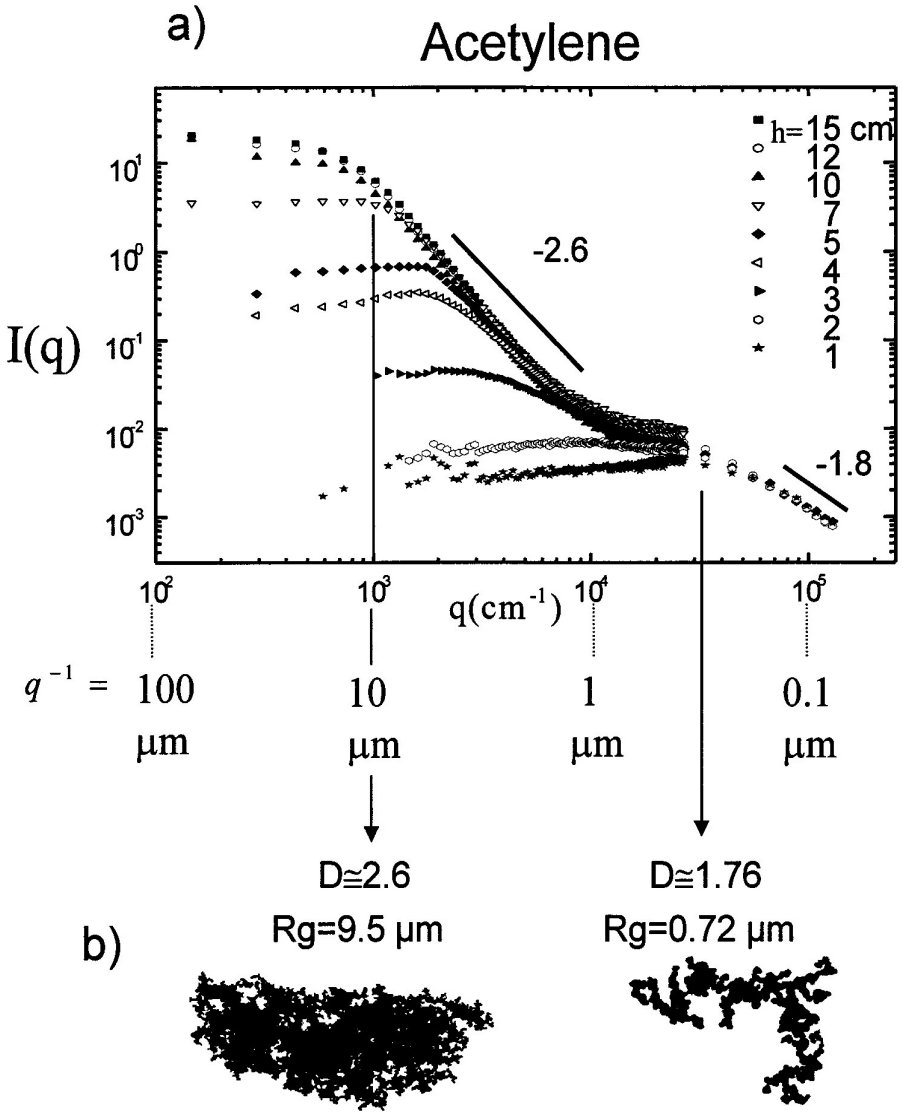

Right side of Fig.2b shows an example of submicrom soot (Stage 1) while left side shows supermicron soot superaggregates (Stage 2).

Similar behavior was observed for Toluene and 1-methylnapthalene.

Fig. 3 Transmission electron micrographs of large soot (supersoot) aggregates.

Next to each image is the perimeter of the aggregate.

Values for the radius of gyration R_g and mass fractal dimension D are given for each cluster. D was determined from the perimeter fractal dimension D_p following Julien, Thouy, and Ehrburger-Dolle (1994).

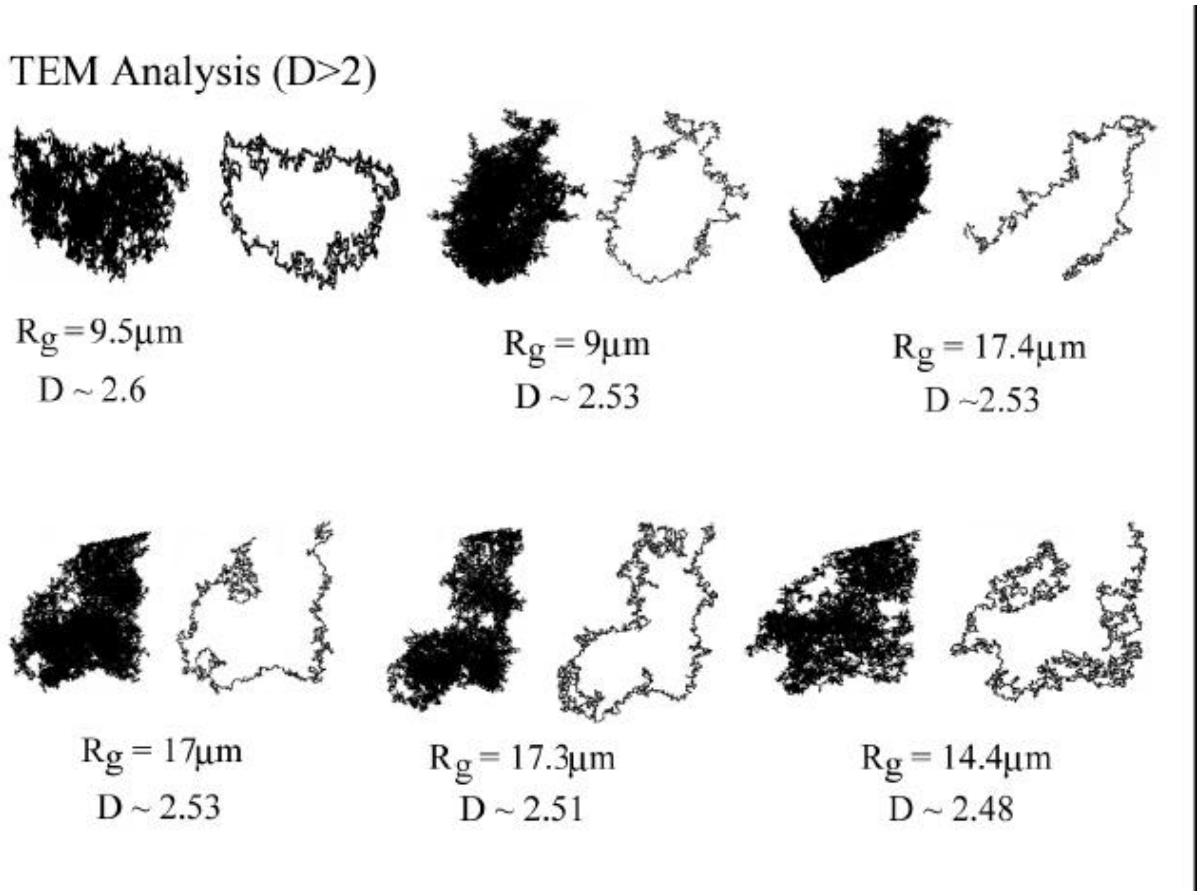

Fig. 4 Structure factor of an off-lattice, DLCA simulation in a cubic box (3d) of side L (measured in primary particle radii a) with N_m primary particles.

The structure factor S(q) is proportional to the light scattered intensity I(q) for a real system.

S(q) evolves with increasing time, as represented by the decreasing number of clusters, N_c, from a system with solely 3d, DLCA, $D \simeq 1.8$ aggregates to a system with percolated superaggregates with $D \simeq 2.6$ composed of the smaller $D \simeq 1.8$ aggregates.

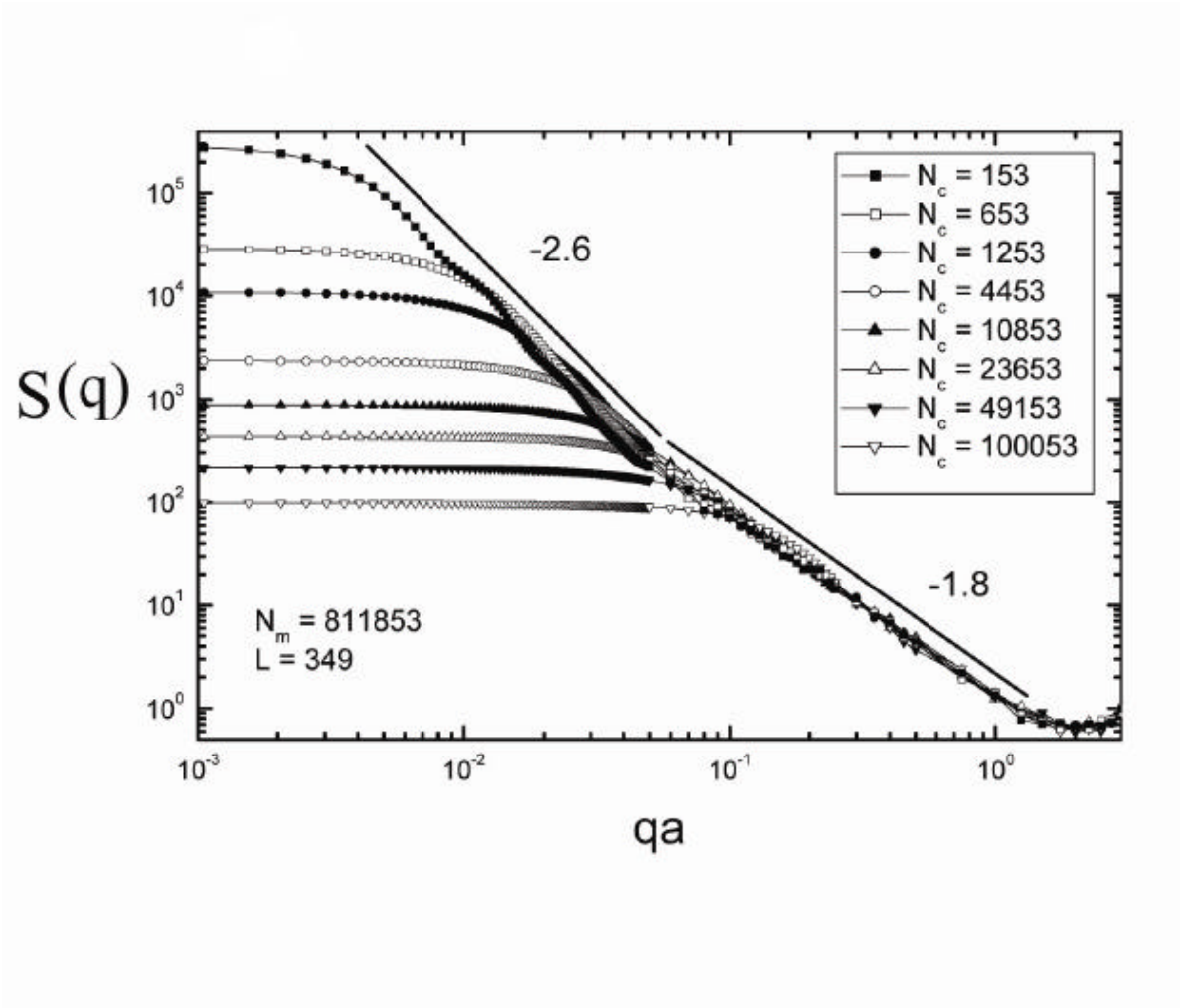

Fig. 5 Diagram of a Superaggregate

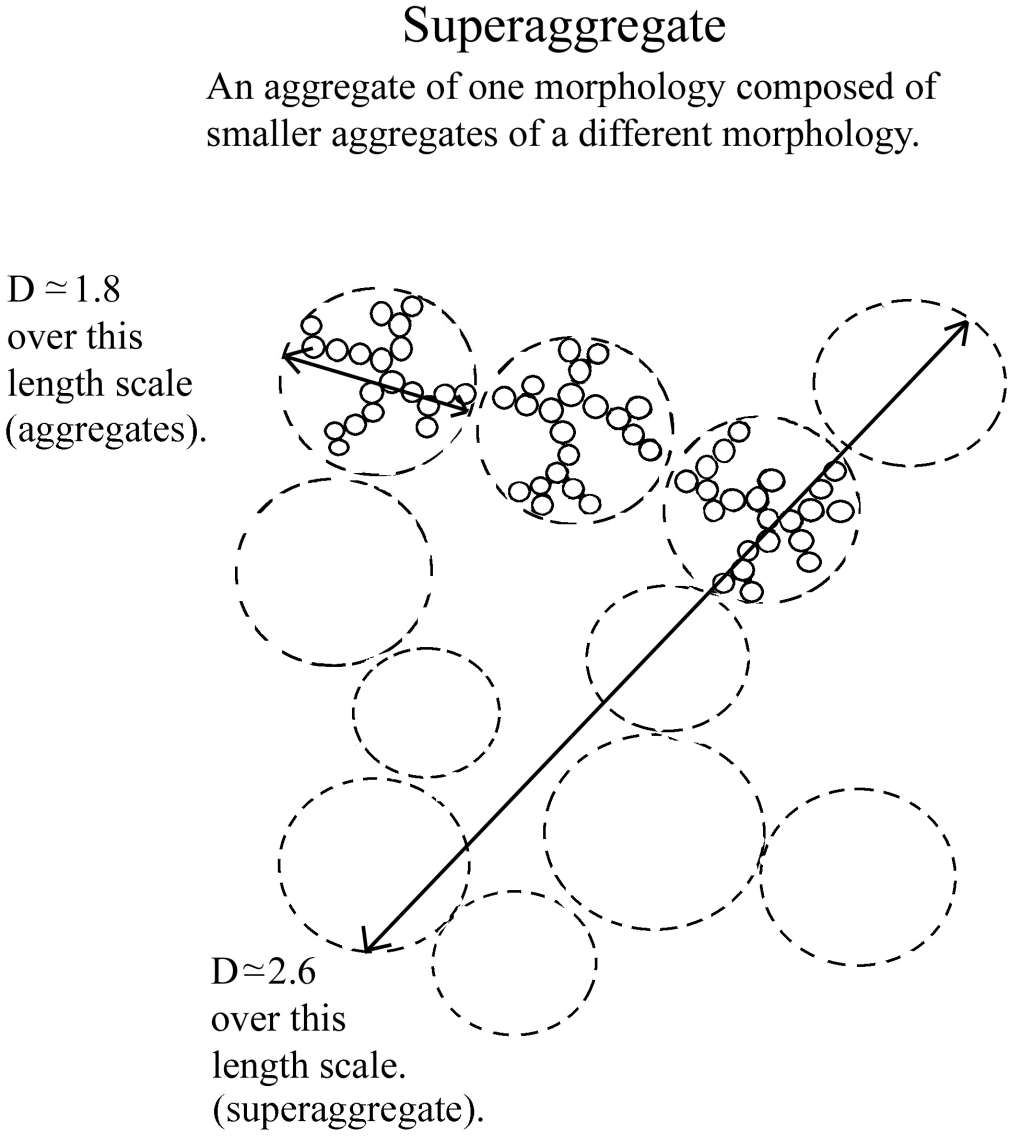

Fig. 6 (a) 7 nsec exposure photograph of soot in an acetylene/air flame at a height above burner of h=10cm. The width of the picture is 1mm.

(b) Binary digitized version of (a).

(c) Number of pixels per aggregate versus radius of gyration for an ensemble of soot clusters including those in (a).

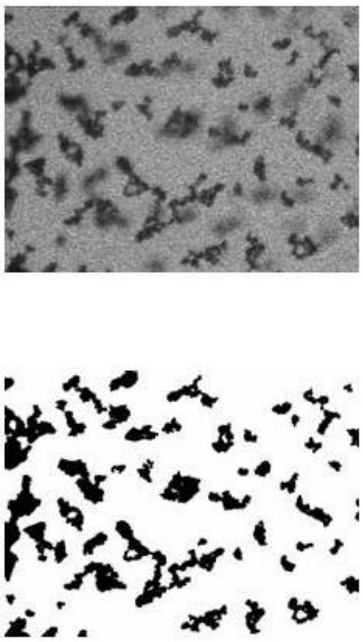

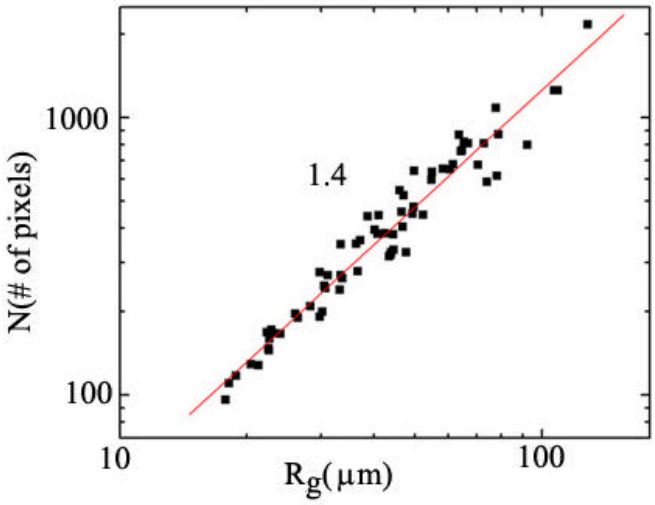

Fig. 7 Fourier transform, hence structure factor S(q), of the digitized image of a flame soot network, lower left corner, in a laminar acetylene/air diffusion flame at a height above burner of h=12cm.

Note the crossover from a slope of ≃ 1.4 to a slope of ≃ 2.1 indicating the formation of a 2d aerogel network.

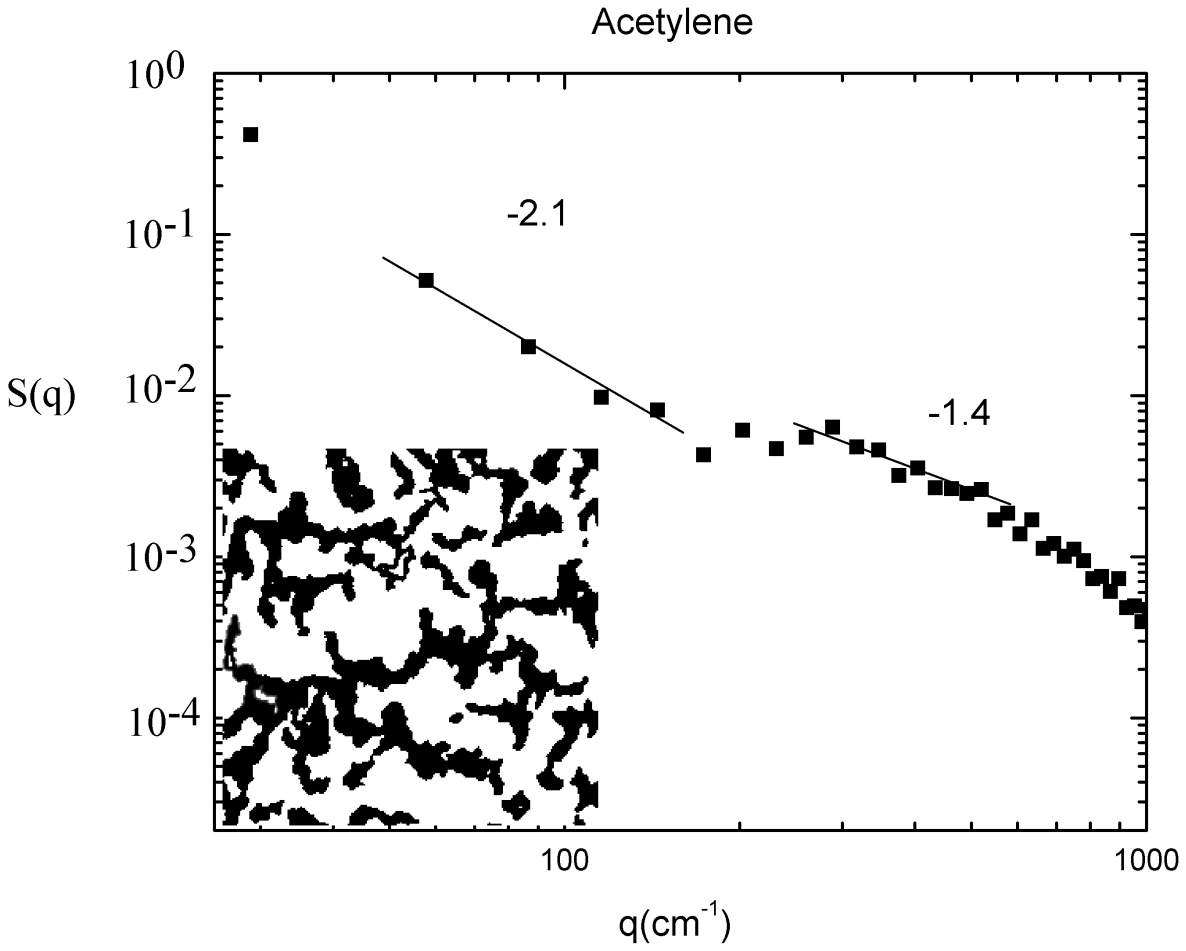

Fig. 8 Structure factor of an off-lattice, DLCA simulation on a square lattice (2d).

The $q^{-3.0}$ regime is the Porod regime of the square box with $q^{-(d+1)}$, d=2 and interference ripples due to the sharp edges of the box.

The $q^{-2.1}$ regime is due to percolated superaggregates with a fractal dimension of 1.9.

The $q^{-1.45}$ regime is due to 2d, DLCA aggregates that make up the superaggregate. The volume fraction of monomers is f_v=0.25.

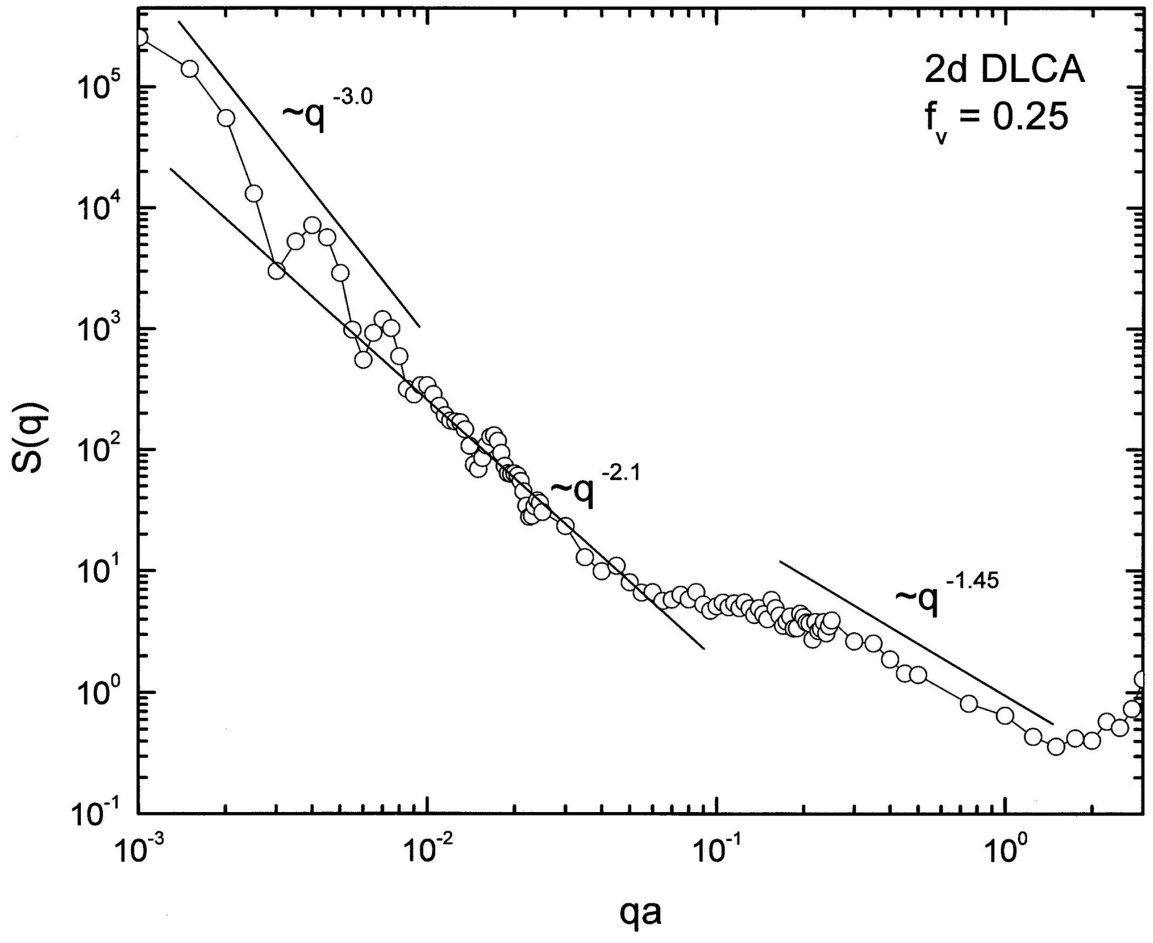

CONCLUSIONS

- **Current work leads to new picture of Soot Morphology in Heavily Sooting Laminar Diffusion Flames.**
- **With increasing Soot aggregate size, a rich phenomenology unfolds.**
- **Four different stages of growth --- each causing a specific morphology in the resulting aggregates.**
- **Summary of Current Work:**

Table I. The Realm of Supersoot

Stage 1	**Stage 2**	**Stage 3**	**Stage 4**
3d DLCA	3d Percolation or Restructuring?	2d DLCA	2d Percolation
$D \simeq 1.8$	$D \simeq 2.6$	$D \simeq 1.4$	$D \simeq 1.9$
aggregates	superaggregates	supersuperaggregates	gel network
$\sim 1mm$	$\sim 10mm$	$\sim 100mm$	

Aggregates and Superaggregates of Soot with Four Distinct Fractal Morphologies

C.M. Sorensen, W. Kim, D. Fry, and A. Chakrabarti

Department of Physics
Kansas State University
Manhattan, KS 66506-2601

The current view of soot formation and growth in flames involves a series of steps including fuel thermal decomposition to small radicals (Palmer and Cullis, 1965; Glassman, 1988) that react to form polyaromatic hydrocarbons (D'Anna, D'Alesso and Minutolo, 1994; Dobbins and Subramaniasivam, 1994; Dobbins, Fletcher and Chang, 1998; Frenklach, 2002) that subsequently nucleate, coalesce and dehydrogenate to yield roughly spherical, graphitic, primary particles of soot with diameters in the few tens of nanometer range (Lahaye and Prado, 1981). After this, the physical process of three-dimensional diffusion limited cluster aggregation (DLCA) (Meakin, 1999; Oh and Sorensen, 1997) proceeds to make noncoalesced clusters which have a fractal morphology with a universal fractal dimension of $D \simeq 1.8$ (Samson, Mulholland and Gentry, 1987; Zhang, Sorensen, Ramer, Olivier and Merklin, 1988; Dobbins and Megaridis, 1990; Sorensen, Cai and Lu, 1992; Koylu and Faeth, 1992). Thereafter environmental restructuring might occur, but with this single step of DLCA, the present description of in-flame soot growth ends.

Our work of the past few years has indicated that this picture is seriously incomplete for the soot produced in heavily sooting laminar diffusion flames. This includes the observation of gel-like networks of soot (Sorensen, Hageman, Rush, Huang and Oh, 1998), flat, two-dimensional soot (Sorensen and Hageman, 2001), and soot with a fractal dimension of 2.6 that was found in a variety of different flames (Sorensen, Kim, Fry, Shi and Chakrabarti, 2003; Kim, Sorensen and Chakrabarti, 2004). In this report we show that with increasing soot aggregate size, a rich phenomenology for soot in these flames unfolds. Four different stages of growth occur each causing a specific morphology in the resulting aggregates. These results are displayed in Table I (of main poster, conclusions section), and the evidence for these results will be described below. Our work is relevant to soot formation in common laminar diffusion flames in which the fuel and the oxidizer (e.g., oxygen in air) flow in a parallel manner in adjacent regions and diffuse together at the flame front.

In our experiments static light scattering was used to measure the structure of the soot aggregates in the flames (Sorensen, 2001). These measurements gave the scattered intensity I(q) as a function of q, the scattering wave vector, $q = 4\pi\lambda^{-1}\sin(\theta/2)$ where λ is the optical wavelength and θ is the scattering angle. An argon ion laser operating at $\lambda = 488\text{nm}$ was used as the light source. Both a small angle apparatus (Ferri, 1997), with $150\ \text{cm}^{-1} \le q \le 2.7\times10^{4}\ \text{cm}^{-1}$ (ca. $0.07^\circ \le \theta \le 12^\circ$) and a large angle apparatus, with $10^{4}\ \text{cm}^{-1} \le q \le 1.4\times10^{5}\ \text{cm}^{-1}$ (ca. $5 \le \theta \le 70^\circ$) were used. A diagram of the apparatus is presented in Fig. 1 (of main poster). Since q^{-1} is the length scale of the scattering experiment, these apparatii allow us to probe soot morphologies from 70nm to nearly $60\mu\text{m}$.

Direct observation of the very large soot in the flame and the flame structure was accomplished using a 10 power photomicroscope with an object distance of 15 cm. The flame was backlit by a 7ns pulsed Nd:YAG laser with $\lambda = 532\text{nm}$ shining on a white background behind the flame. The flames were all laminar diffusion flames in ambient air. Gaseous fuels at controllable flow rates emanated from a brass tube 0.9 cm inside diameter. Liquid fuels were burned with a simple wick burner with wick diameter of 0.6 cm. Solid naphthalene was molded into a candle 0.6 cm in diameter. The fuels used are listed in Table 2 below.

Figure 2a of main poster shows the scattered intensity as a function of the wavevector, I(q), for an acetylene flame. Low in the flame, i.e., for heights above burner of h<2cm, the scattering is isotropic for low q but then bends over to a power law with slope ca. -1.8. The bend occurs near $q \simeq 3\times10^{4}\ \text{cm}^{-1}$ to imply an aggregate size of $q^{-1} \simeq 0.3\mu\text{m}$. This corresponds to the often observed and well known phase of submicron, fractal dimension $D \simeq 1.8$ soot which is a result of a 3d DLCA aggregation process (Meakin, 1999; Oh and Sorensen, 1997) (stage 1, Table 1).

Table 2. Fuels, threshold soot indices (TSI), and measured fractal dimensions within the 4 stages of soot growth. Dash means no measurements were attempted although stage 1 is expected for all flames.

Fuel	TSI	Stage 1	Stage 2	Stage 3	Stage 4
Gases					
Methane	~0	1.8	No	No	No
Ethylene	0.7	1.8	No	No	No
Acetylene	11	1.7	2.7	1.44	1.9
Liquids					
Hexadecane	5.8	-	No	No	No
Isooctane	6.4	-	No	No	No
1-Hexadecene	11	-	No	No	No
JP5 Fuel	-	-	Marginal	No	No
Decaline	15	-	Marginal	No	No
Toluene	44	1.7	2.6	1.39	1.9
Styrene	67	-	2.6	-	-
1-Methyl Naphthalene	91	1.8	2.5	(1.4)	1.9
Solid					
Naphthalene	100	-	2.7	1.5	1.9

With increasing height above burner, which corresponds to increasing time for the soot to grow, a very intense, second phase appears at low q. In the region ca. $800 \le q \le 8000\ cm^{-1}$ the slope of the log-log plot indicates a power law $I(q) \sim q^{-2.6}$ for this second phase. Note that the $q^{-1.8}$ regime remains at large q. This scattering behavior may be interpreted to indicate a phase of ca. $12\mu m$ soot with a fractal dimension of $D \simeq 2.6$ for length scales of $1.2\mu m$ to $12\mu m$ (stage 2) and $D \simeq 1.8$ for scales smaller than $0.3\mu m$ down to the primary particle size (ca. 25nm as determined by TEM). Results for the toluene and 1-methylnaphthalene show the same behavior. We have shown (Kim, Sorensen and Chakrabarti, 2004) that this large, $D \simeq 2.6$ phase occurs in laminar diffusion flames of all heavily sooting fuels as quantified by the Thermal Sooting Index (TSI) as defined by Calcote and Manos, 1983 and Olson, Pickens and Gill, 1985, specifically when $TSI \ge 10 \pm 2$ (roughly, the larger the fuel TSI, the sootier the flame). Otherwise, for less sooty flames only the submicron, $D \simeq 1.8$ soot is seen; no $D \simeq 2.6$ phase nor the subsequent phases to be described below (see Table 2).

To corroborate the light scattering measurements soot was sampled from the flame using a well established thermophoretic technique (Dobbins and Megaridis, 1987). Figure 2b (right side) shows an example of submicron soot (stage 1) collected low in the acetylene/air diffusion flame and Fig. 2b (left side) shows an example of supermicron soot superaggregates (stage 2) collected high in the flame. Visual inspection shows the much more compact appearance of the large soot than the small, qualitatively supporting a larger fractal dimension for the larger aggregate. Previous real space analysis of projected images of submicron soot have confirmed the $D \simeq 1.7$ to 1.8 fractal dimension (Dobbins and Megaridis, 1987; Koylu and Faeth, 1992; Cai, Lu and Sorensen, 1993).

For the large soot aggregates we applied an analysis developed by Jullien, Thuoy and Ehrburger-Dolle, 1996 for 2d projected images of 3d fractal aggregates with D>2. Using simulations they found the relation $D = 3 - (D_p - 1)^{2/3}$ between the perimeter fractal dimension D_p and the true 3d mass fractal dimension D. Figure 3 in the main poster gives more examples of these large, relatively dense soot aggregates. We measured 10 large clusters to find $D_p = 1.26 \pm 0.06$. This D_p implies $D = 2.6 \pm 0.06$, in excellent agreement with our light scattering results. Furthermore, the average size we measure for the collected aggregates is $10 \pm 3\mu m$, also in excellent agreement with light scattering.

The mechanism that creates this second phase is still somewhat uncertain. One scenario is that it represents 3d DLCA clusters with initial $D \simeq 1.8$ that have grown to ca. $10\mu m$ or larger and then restructured to a denser $D \simeq 2.6$ (hence smaller) under the shear stress at the flame front. There is evidence for shear restructuring of

DLCA aggregates to larger fractal dimensions in colloids (Martin, Wilcoxon and Schaefer, 1990; Carpeneti, 1990; Jung, Amal and Raper, 1996; Selomulya, Bushell, Amal and Waite, 2002). There is, however, no evidence for ca. $10\mu m$, $D \simeq 1.8$ aggregates in our flames necessary for restructuring. A second scenario, that we consider more likely and have described previously (Sorensen, Kim, Fry, Shi and Chakrabarti, 2003; Kim, Sorensen and Chakrabarti, 2004; Fry, Chakrabarti, Kim and Sorensen, 2003), was inspired by our recent simulations (Fry, Chakrabarti, Kim & Sorensen, 2003) of 3d DLCA that show when the aggregates grow, they eventually fill all space and then jam together. The result is a percolated, $D \simeq 2.6$ *superaggregate* of the smaller $D \simeq 1.8$, DLCA aggregates. Structure factors of our simulations, Fig. 4 is an example, show both the $D \simeq 2.6$ and $D \simeq 1.8$ regimes as seen in our flame data, e.g., Fig. 2a. We have shown that the crossover length scale between the $D \simeq 1.8$ and 2.6 regimes is consistent with soot volume fraction measurements (Sorensen, Kim, Fry and Chakrabarti, 2003; Fry, Chakrabarti, Kim and Sorensen, 2003, Fry, Sintes, Chakrabarti and Sorensen, 2002). Figure 5 shows a diagram of our vision of a superaggregate.

Figures 6a shows 7nsec exposure photographs of submillimeter soot in acetylene. These clusters are flat, quasi-2d (they are seen face on in Figs. 6a) similar to those seen previously in acetylene flames (Sorensen and Hageman, 2001) (stage 3). Following that previous analysis, cluster images were digitized into binary format (Figs. 6b) then were analyzed to determine the number of dark pixels N_p, which is proportional to cluster mass, and R_g, the cluster radius of gyration for each cluster. If the clusters are fractal, then the well known relationship $N_p \sim R_g^D$ will hold. Figures 6c shows a log-log plot of N_p vs. R_g yielding a fractal dimension of $D = 1.44 \pm 0.05$. Thus flames yield flat aggregates with a fractal dimension of ca. 1.45 over length scales of ca. 10 to $100\mu m$. This morphology is stage 3 in Table 1. Similar results were found previously (Sorensen and Hageman, 2001).

In previous work on laminar acetylene/air flames we concluded that this phase of soot occurs because the soot, which is confined to an annular flame front, becomes larger than the thickness of the flame front and thus is confined in an effectively two-dimensional (2d) space (Sorensen and Hageman, 2001) in which to aggregate. Simulations of 2d DLCA yield fractal aggregates with D=1.44 consistent with our measurements (Meakin, 1999). Thus we named this phase "two-dimensional soot." Since this phase of soot is immediately larger than the second phase of soot described above, and since it has a different fractal dimension, 1.45 as opposed to 2.6, we propose that it is a third phase of soot consisting of 2d, DLCA aggregates of the superaggregates of phase two. We call these aggregates of superaggregates "supersuperaggregates." They have three levels of structure, each level having its own fractal dimension, and two crossover length scales, one between each consecutive level, as outlined in Table 1, stages 1, 2, and 3.

Flame spanning networks of soot are seen higher in the flames or at larger fuel flow rates. Example of a digitized image for acetylene flames is given in the lower left hand corner of Fig. 7. Once again we stress that as for the supersuperaggregates these networks are confined to the thin cylindrical annulus of the flame front. In previous work we argued that this network was an aerogel (Sorensen, Hageman, Rush, Huang and Oh, 1998), an argument that we will now support quantitatively. Analysis of this aerogel network structure was accomplished by Fourier transformation of the digitized images obtained with the photomicroscope. Analysis of Fourier transform data at low q is hampered by the finite size of the picture that is 1mm square. The raw data show "interference ripples" due to the hard edges of the picture box. To remove this box effect the uniform box was Fourier transformed, and the raw data were normalized with this to yield a corrected structure factor showing only the structure of the image, not the picture box. The resulting q-space function is a structure factor, S(q) vs. q, is proportional to a light scattering result, I(q), shown in Fig. 7.

In each analysis at large $q\left(>1000cm^{-1}\right)$ a slope of -3 is found (not shown in the figures) We interpret this as Porod scattering, $I(q) \sim q^{-(d+1)}$ for d=2, to imply that the image is uniformly black for lengths $q^{-1} < 10^{-3} = 10\mu m$. This value is consistent with our photographic resolution limit which we estimate to be $5\mu m$, i.e., for length scale less than 5 to $10\mu m$ the image is uniformly black and two dimensional. This is a mild test of our analysis.

For $200 \le q \le 700cm^{-1}$, which corresponds to length scales q^{-1} of 14 to $50\mu m$, the I(q) data roughly follow a power law of $I(q) \sim q^{-1.4}$. This is a poor resolution observation of a remnant of the 2d, $D \simeq 1.45$ supersuperaggregates, stage 3. We propose that it is these supersuperaggregates that come together to form the gel network. For $30 \lesssim q \lesssim 200\ cm^{-1}$, i.e., length scales of 50 to $300\ \mu m$, data for all flames showed a $I(q) \sim q^{-2.1}$ power law. This power law can be understood by comparing to simulations of 2d DLCA aggregation we performed. These simulations were allowed to proceed until the system percolated to form a gel network. Figure 8 shows the

structure factor for a simulation with nearly 4×10^5 monomers allowed to aggregate via Brownian motion in a 2d box until only one large cluster formed. Real space analysis of this large cluster showed it had a fractal dimension of 1.9, consistent with a 2d, percolation cluster (Stauffer and Aharony, 1992). The entire box was Fourier transformed for direct comparison to the flame network data. The results in Fig. 14 are strikingly similar to the flame data including both the $q^{-1.4}$ and $q^{-2.1}$ regimes (and interference ripples due to the finite system size). The power law exponent (2.1) does not equal the fractal dimension, $D\simeq1.9$, in this case because D is almost equal to the spatial dimension d. Note that when D=d, a Porod law with power –(d+1) results, which would be q^{-3} for this 2d situation. Thus the $q^{-2.1}$ power law implies that the fractal dimension of the network, in both the flame soot and the simulation, is less than but very close to the spatial dimension of d=2. This strongly supports the contention that the gel-like network structure in our flames is the result of a 2d percolation of the $D\simeq1.4$, 2d DLCA, supersuperaggregates.

ACKNOWLEDGMENT

This work was supported by NSF grant CTS0080017 and NASA grant NAG3-2360.

REFERENCES

1. Cai, J., Lu, N. & Sorensen, C. M. (1993), *Langmuir, **9**,* 2861-2867.
2. Calcote, H. F. & Manos, D. M. (1983), *Combust. Flame, **49**,* 289-304.
3. Carpineti, M., Ferri, F., & Giglio, M. (1990), *Phys. Rev. A, **42**,* 7347-7354.
4. D'Anna, A., D'Alesso, A. & Minutolo, P. (1994), in H. Bockhorn (Ed), *Soot Formation in Combustion: Mechanisms and Models* (p. 83), Springer-Verlag, Heidelberg.
5. Dobbins R. A. & Megaridis, C. M. (1987), *Langmuir, **3**,* 254-259.
6. Dobbins, R. A. & Megaridis, C. M. (1990), *Combust. Sci. Tech., **71**,* 95-109 .
7. Dobbins R. A. & Subramaniasivam, H. (1994), Soot precursor Particles in Flames, in H. Brockhorn (Ed.), *Soot Formation in Combustion: Mechanisms and Models* (pp. 290-301), Springer-Verlag Berlin, Heidelberg,.
8. Dobbins, R. A., Fletcher, R. A. & Chang, H.-C. (1998), *Comb. & Flame, **115,*** 285-298.
9. Ferri, F. (1997), *Rev. Sci. Instr., **68,*** 2265-2274.
10. Frenklach, M. (2002), *Phys. Chem. Chem. Phys., **4**,* 2028-2037.
11. Fry, D., Sintes, T., Chakrabarti, A. & Sorensen, C. M. (2002), *Phys. Rev. Lett., **89,*** 148301-148301-4.
12. Fry, D., Chakrabarti, A., Kim W. & Sorensen C. M. (2004), *Phys. Rev. E, **69**,* 061401-1-061401-10.
13. Glassman, I. (1988), Soot formation in combustion processes; *Twenty-Second Symposium (International) on Combustion* (pp. 295-311), The Combustion Institute.
14. Jullien, R., Thouy, R. & Ehrburger-Dolle, F. (1994), *Phys. Rev. E, **50,*** 3878-3882.
15. Jung, S. J., Amal, R. & Raper, J. A. (1996), *Powder Tech. **88**,* 51-54.
16. Kim, W., Sorensen, C. M. & Chakrabarti, A. (2004), **20**, 3969-3973.
17. Koylu, U. O. & Faeth, G. M. (1992), *Combust. Flame, **89,*** 140-156.
18. Lahaye J. & Prado, G. (1981), Morphology & internal structure of soot & carbon blacks, in D.C. Siegla, and G.W. Smith (Eds.), *Particulate carbon: Formation during combustion* (pp. 33-51); Plenum Press, New York.
19. Martin, J. E., Wilcoxon, J. P., Schaefer, D. & Odinek, J. (1990), *Phys. Rev. A, **41**,* 4379-4391.
20. Meakin, P. (1999), *J. of Sol-Gel Sci. & Tech., **15**,* 97-117.
21. Oh, C. & Sorensen, C.M. (1997), *J. Aerosol Sci., **28**,* 937-957.
22. Olson, D. B. Pickens, J. C. and Gill, R. J. (1985), *Combust. Flame, **62,*** 43-60.
23. Palmer, H. B. & Cullis H. F. (1965), *The Chemistry and Physics of Carbon*, Vol. 1, 205, Marcel Dekker, New York.
24. Samson, R. J., Mulholland, G. W., & Gentry, J. W. (1987), *Langmuir, **3,*** 272-281.
25. Selomulya, C., Bushell, G., Amal, R. & Waite, T.D. (2002), *Langmuir, **18,*** 1974-1984.
26. Sorensen, C. M., Cai, J. & Lu, N. (1992), *Appl. Optics, **31,*** 6547-6557.
27. Sorensen, C.M., Hagemann, W.B., Rush, T.J., Huang, H. & Oh, C. (1998), *Phys. Rev. Lett., **80,*** 1782-1785.
28. Sorensen, C. M. & Hageman, W.B. (2001), *Langmuir, **17,*** 5431-5434.
29. Sorensen, C. M. (2001), *Aerosol Sci. Tech., **35,*** 648-687.
30. Sorensen, C. M., Kim, W., Fry, D., Shi, D. & Chakrabarti A. (2003), *Langmuir, **19**,* 7560-7563.
31. Stauffer, D. & Aharony, A. (1992), *Introduction to Percolation Theory*, Taylor and Francis, London.
32. Zhang, H. X., Sorensen, C. M., Ramer, E. R., Olivier, B. J. & Merklin, J. F. (1988), *Langmuir, **4**,* 867-871.